scientific reports

OPEN

Breaking the hard-sphere model with fluorite and antifluorite solid solutions

Romain Vauchy[1]✉, Shun Hirooka[1], Masashi Watanabe[2] & Masato Kato[1,2]

Using the hard-sphere model with the existing tabulated values of ionic radii to calculate the lattice parameters of minerals does not always match experimental data. An adaptation of this crystallographic model is proposed by considering the cations and anions as hard and soft close-packed spheres, respectively. We demonstrate the relevance of this "hybrid model" by combining Pauling's first rule with experimental unit-cell parameters of fluorite and antifluorite-structured systems to revise the ionic radii of their constitutive species.

Ionic crystals are the alternate and periodic stacking of cations and anions forming a structural lattice by the balance between their attractive and repulsive forces. In the hard-sphere model, these ions are in contact and their radii are reported to depend on their oxidation state and coordination number (noted C.N.)[1]. Assessing these solids' lattice parameters from the ionic radii of the constitutive species is paramount to understanding their defect chemistry and/or variations in their composition. Pauling proposed five empirical rules that these crystals shall respect to be stable[2]. The first stipulates that the coordination number of the cation depends on the ionic radii ratio r_{cation}/r_{anion} and that the latter should range between specific values determined by geometry construction; otherwise, the structure is unstable, and the coordination changes. Shannon[3] highlighted that using the tabulated ionic radii to model such materials' lattice structures does not always match the experimental values and/or Pauling's rules. Some studies also propose revised ionic radii[4] that better agree with diffraction experiments; however, they do not coincide with the geometrical criteria.

Fluorites and antifluorites are critical ionic solids for a myriad of applications such as catalysts[5], electroceramics[6], or even nuclear fuels[7], and thanks to their high symmetry, their geometry is simple to model (Fig. 1). Their lattice parameter *a* can be calculated using Eq. 1 from the body diagonal of the lattice (cube) and the ionic radii *r* of the constitutive species.

$$a = \frac{4}{\sqrt{3}} \times (r_{cation} + r_{anion}) \tag{1}$$

The cations and anions are in 8- and fourfold coordination in fluorites, respectively. The structure is stable if $0.732 \leq r_{cation}/r_{anion} \leq 1.000$[8]. Since antifluorite is the fluorite's antistructure, these ions' positions are permuted and the crystallographic arrangement is stable if $0.225 \leq r_{cation}/r_{anion} \leq 0.414$[8]. These structures were widely studied in the past century and experimental lattice parameters are numerous. At the light of these crystals, we break the hard-sphere model by demonstrating that anions are soft because their ionic radius not only depends on their charge and coordination number but also on the nature (thus size) of the closest neighbors.

Ideal fluorites & antifluorites

Table 1 shows Shannon's[1] ionic radii of the constitutive species of some selected important compounds for their use in various fields (fluorites: ZrO_2, TbO_2, HfO_2, CeO_2, ThO_2, UO_2, NpO_2, PuO_2, AmO_2, CmO_2, BkO_2, CfO_2, CaF_2, SrF_2, BaF_2, EuF_2, and PbF_2; antifluorites: Na_2O, Li_2O, and K_2O). The associated r_{cation}/r_{anion} ratios, compared to the stability criteria of Pauling's first rule, and their experimental lattice parameters at room temperature obtained using diffraction methods are also listed.

First of all, the difference in Pauling's electronegativity $\chi_{anion} - \chi_{cation}$ in the selected compounds is larger than the minimum value of ~ 1.7 that defines the ionic solids[8,9]. Indeed, $\Delta\chi$ ranges between 2.06 (UO_2) and 3.09

[1]Plutonium Fuel Development Center, Japan Atomic Energy Agency, 4-33 Muramatsu, Tōkai-Mura, Ibaraki 319-1194, Japan. [2]Nuclear Plant Innovation Promotion Office, Japan Atomic Energy Agency, 4002 Narita-Cho, Ōarai-Machi, Ibaraki 311-1393, Japan. ✉email: vauchy.romain@jaea.go.jp

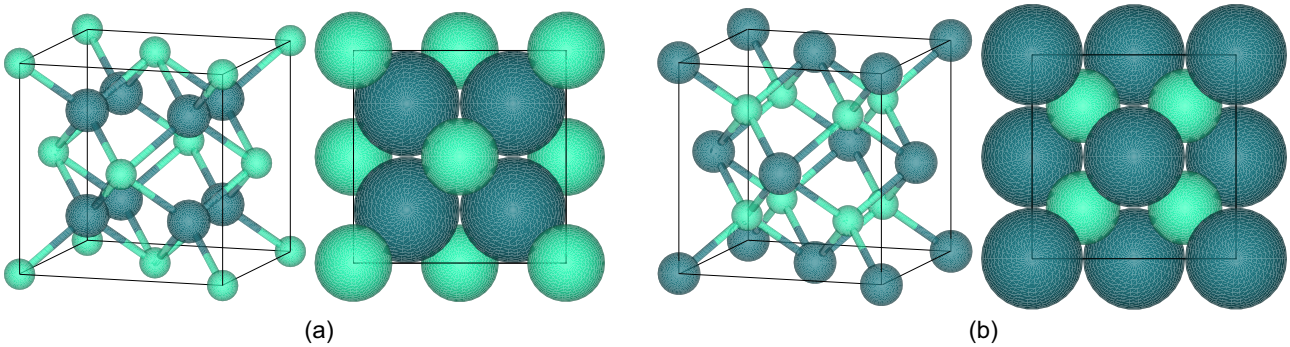

Figure 1. Unit-cell drawings of ideal (**a**) fluorite and (**b**) antifluorite structures and their respective projections (space-filling spheres) along the (100) plane. The small ocean-mint and large petrol-blue spheres represent the cations and anions, respectively.

Structure	Compound	Ionic species	C.N	Ionic radius (Å)[1]	r_{cation}/r_{anion}	Lattice parameter (Å) at 298 K	Pauling's electronegativity χ[9]	$\chi_{anion} - \chi_{cation}$
Fluorite	–	O(−II)	4	1.38	–	–	3.44	–
	ZrO_2	Zr(IV)	8	0.84	~ **0.609**	5.135(5)[10]	1.33	2.11
	TbO_2	Tb(IV)	8	0.88	~ **0.638**	5.213(2)[11]	1.20	2.24
	HfO_2	Hf(IV)	8	0.83	~ **0.601**	5.115[12]	1.30	2.14
	CeO_2	Ce(IV)	8	0.97	~ **0.703**	5.411(1)[13]	1.12	2.32
	ThO_2	Th(IV)	8	1.05	~ *0.761*	5.5971(5)[14]	1.30	2.14
	UO_2	U(IV)	8	1.00	~ **0.723**	5.47127(8)[15]	1.38	2.06
	NpO_2	Np(IV)	8	0.98	~ **0.710**	5.4336(5)[14]	1.36	2.08
	PuO_2	Pu(IV)	8	0.96	~ **0.696**	5.3954(5)[16]	1.28	2.16
	AmO_2	Am(IV)	8	0.95	~ **0.688**	5.3755(5)[16]	1.13	2.31
	CmO_2	Cm(IV)	8	0.95	~ **0.688**	5.3598(4)[17]	1.28	2.16
	BkO_2	Bk(IV)	8	0.93	~ **0.674**	5.3304(8)[18]	1.30	2.14
	CfO_2	Cf(IV)	8	0.92	~ **0.667**	5.310(2)[19]	1.30	2.14
	-	F(−I)	4	1.31	–	–	3.98	–
	CaF_2	Ca(II)	8	1.12	~ *0.855*	5.4779(4)[20]	1.00	2.98
	SrF_2	Sr(II)	8	1.26	~ *0.962*	5.8771(7)[20]	0.95	3.03
	BaF_2	Ba(II)	8	1.42	~ 1.084*	6.200(1)[21]	0.89	3.09
	EuF_2	Eu(II)	8	1.25	~ *0.954*	5.808[22]	1.20	2.78
	PbF_2	Pb(II)	8	1.29	~ *0.985*	5.940(1)[23]	1.87	2.11
Antifluorite	-	O(−II)	8	1.42	–	–	3.44	–
	Na_2O	Na(I)	4	0.99	~ **0.697**	5.544(2)[24]	0.93	2.51
	Li_2O	Li(I)	4	0.59	~ **0.415**	4.6117(5)[25]	0.98	2.46
	K_2O	K(I)	4	1.37	~ **0.993**	6.436[26]	0.82	2.62

Table 1. Calculated r_{cation}/r_{anion} ratios from Shannon's ionic radii[1] of selected fluorite and antifluorite-structured compounds and their experimental lattice parameters at room temperature determined using X-ray diffraction. *BaF_2 is a peculiar example as the cation is larger than the anion ($r_{cation}/r_{anion} > 1$). From a geometrical stability point of view, it shall be considered as an antifluorite as the smaller ion is in fourfold coordination instead of 8. The ratios highlighted in italic and bold correspond to the structures that respect and violate Pauling's first rule, respectively. Pauling's electronegativity χ[9] values and $\chi_{anion} - \chi_{cation}$ are also listed.

(BaF_2). Discussing the ionic radii of the constitutive species is then legitimate and the high ionicity of the bonds allows approximating ions as spherical entities.

The compounds highlighted in bold in Table 1 should not be stable if the r_{cation}/r_{anion} lower limit of Pauling's first rule is respected or if Shannon's ionic radii are correct. To fulfill the geometric stability criteria and to match the experimental unit-cell measurements of these ionic crystals, we consider the anions as soft spheres with an effective radius varying as a function of the cation's nature by deriving Eq. (1) in Eq. (2).

$$r_{anion} = a \times \frac{\sqrt{3}}{4} - r_{cation} \quad (2)$$

In the peculiar case of the fluorites highlighted in bold in Table 1, the r_{cation}/r_{anion} ratio is smaller than the lower stability limit, so cations and anions are not in contact in this configuration. The unit-cell is a close-packed arrangement of anions and can be calculated using Eq. 3.

$$a = 4 \times r_{anion} \quad (3)$$

If a fixed anionic radius is considered, these compounds' lattice parameters will also be, geometrically, independent of the nature of the cations that partly fill the interstices of the structure (Fig. 1). However, this is not verified experimentally, as evidenced by the variations in the lattice parameters observed when the cation is changed (Table 1). The cations and anions shall be, at least, in contact one another[2]. Thus, from the accurate experimental lattice parameters, applying Eq. (3) to UO_2 and PuO_2 gives two oxygen radii of 1.368 and 1.349 Å, respectively. Implementing these values in Eq. (2) allows determining the revised cation radii giving 1.001 and 0.987 Å for U(IV) and Pu(IV) in 8-coordination, respectively. Similarly, the constitutive species' ionic radii of the bold fluorite compounds in Table 1 were re-evaluated (Table 3 in supplementary materials).

UO_2 and PuO_2 are known to form a solid solution of $U_{1-y}Pu_yO_2$, i.e., U and Pu can be substituted in their mutual lattice. When the two oxygen ionic radii are individually used to plot the theoretical Vegard's law between UO_2 and PuO_2, no value matches the experimental variations in the fluorite structure's lattice parameter as a function of the Pu content, *y* (Fig. 2a). As the commuted species, U and Pu do not have the same ionic radii, the crystal's geometry is locally deformed. Since the ions are considered contacted spheres, the cation–anion distance will change when incorporating the doping species in the host lattice. To do so, and by considering the anions as a close-pack arrangement, the r_{anion} will vary proportionally to the incorporation of the doping cation within the lattice. Figure 2b plots the variations in the oxygen ion size as a function of the plutonium concentration in the $U_{1-y}Pu_yO_2$ solid solution from the linear regression between UO_2 and PuO_2. This model allows reproducing of the experimental lattice parameters of $U_{1-y}Pu_yO_2$ and matches the geometrical criteria established by Pauling.

As antifluorites are the antistructure of fluorites, the same method can be used to estimate their solid solutions' lattice parameters from the pure constitutive poles.

If the coordination number and the oxidation state of the considered cations do not change, this method could be used for any ionic crystal and predict the lattice parameters of solid solutions not yet investigated experimentally, as long as the difference in cations' electronegativity, $\Delta\chi_M$, is small. Indeed, a large $\Delta\chi_M$ results in a disordered structure due to the resulting different Cation–Anion bond distances. Ultimately, the gradual incorporation of a dopant element within the host lattice changes the local coordination number of one of the cations, even if they have identical oxidation sates and comparable ionic radii[27].

Incorporating aliovalent cations

Doping is widely used for tailoring a given material's properties (optical, electrical, redox). Aliovalent atoms are frequently used as dopants to boost the target properties. Also, some cations can have various oxidation states within the same structure, resulting in a deviation from stoichiometry. Due to their exceptional aptitude to form solid solutions, fluorites and antifluorites are often doped, even with aliovalent cations, and can likewise be subjected to dramatic variations in stoichiometry[7,16] and/or complex charge compensation processes[28]. Such

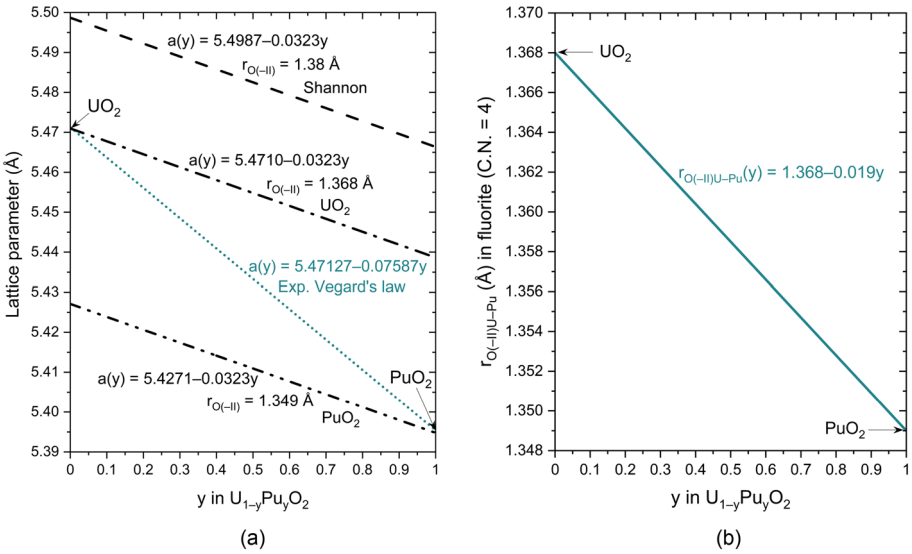

Figure 2. Variations in (**a**) experimental lattice parameter of $U_{1-y}Pu_yO_2$ at room temperature as a function of y (petrol-blue dotted line) compared with calculations (Eq. 1) from the hard-sphere model with three oxygen ionic radii (black dashed lines) and (**b**) the ionic radius of oxygen as a function of y, noted $r_{O(-II)U-Pu}$.

intrusive atoms generate lattice distortions and/or crystal defects, and the ratio of the ionic radii of the two permuted atoms will be considered to evaluate the effect of such a dopant on the host structure's lattice parameters.

However, using our method in such materials might be problematic because one of the pure poles might crystallize in a different structure than the host lattice. For instance, in Nd-doped UO_2 fluorite, neodymium is trivalent, and its oxide form is Nd_2O_3 (either cubic or haxagonal[29]); thus, a direct application of our method cannot estimate the variations in the oxygen radius with the Nd concentration in $U_{1-y}Nd_yO_2$. Therefore, we propose an alternate method that compares the fluorite/nonfluorite pseudo-binary system to a known fluorite/fluorite couple. Hence, our UO_2/Nd_2O_3 example can be paralleled to the well-known UO_2/PuO_2 system by comparing the sizes of Pu(IV) and Nd(III) ions in eightfold coordination. Also, doping UO_2 with trivalent neodymium should be balanced by a partial oxidation of uranium to its pentavalent state in the same proportions as the Nd incorporation[30]. Thus, the size of U(V) will be considered. Table 2 presents the ionic radii of the constitutive cations (C.N. = 8) and the associated $r_{cation}/r_{Pu(IV)}$ ratios.

Figure 3a plots the variations in the experimental lattice parameters of $U_{1-y}M_yO_2$ as a function of the dopant content y with M = Pu[16,33–36] or Nd[30,31,37–39], and (b) represents the calculated theoretical lattice parameters of $U_{1-y}Nd_yO_2$ from the ionic radii ratios of Table 2.

The exquisite agreement between the experimental and calculated lattice parameters of $U_{1-y}Nd_yO_2$ represented in Fig. 3b confirms that: (1) the theoretical crystallography calculations verify that the Nd(III)/U(V) charge compensation model in $U_{1-y}Nd_yO_2$ is correct, and (2) our geometrical hybrid model based on the parallelism between the considered fluorite/nonfluorite system to a known fluorite/fluorite one is successful. However, one may keep in mind that the disorder generated by the incorporation of a dopant cation (aliovalent or not) within the lattice may affect the unit-cell parameters, inducing deviations from the pseudo-Vegard's law[40].

Similarly, the investigation of higher-order systems is possible. For example, stoichiometric $U_{1-y}M_yO_2$ with M = Pu + Am is a complex system where americium can take a pure tetravalent oxidation state, a mixed Am(III)/Am(IV) valence, or be purely trivalent depending on its concentration and distribution homogeneity[41]. Likewise, Am(III) in uranium–plutonium–americium mixed oxides is balanced by U(V)[28], but a clear trend regarding the

Ionic species	Ionic radius r (Å)	$r_{cation}/r_{Pu(IV)}$ (%)
U(V)	0.88[31]	− 10.84
U(IV)	~ 1.001[32]*	+ 1.42
Pu(IV)	~ 0.987[32]**	–
Nd(III)	1.109[1]	+ 12.36

Table 2. Ionic radii ratios $r_{cation}/r_{Pu(IV)}$ of the doping species in fluorite Nd- and Pu-doped UO_2. *Calculated with a_{UO_2} equal to 5.47127(8) Å at 298 K[15]. **Calculated with a_{PuO_2} equal to 5.3957(5) Å at 298 K[16].

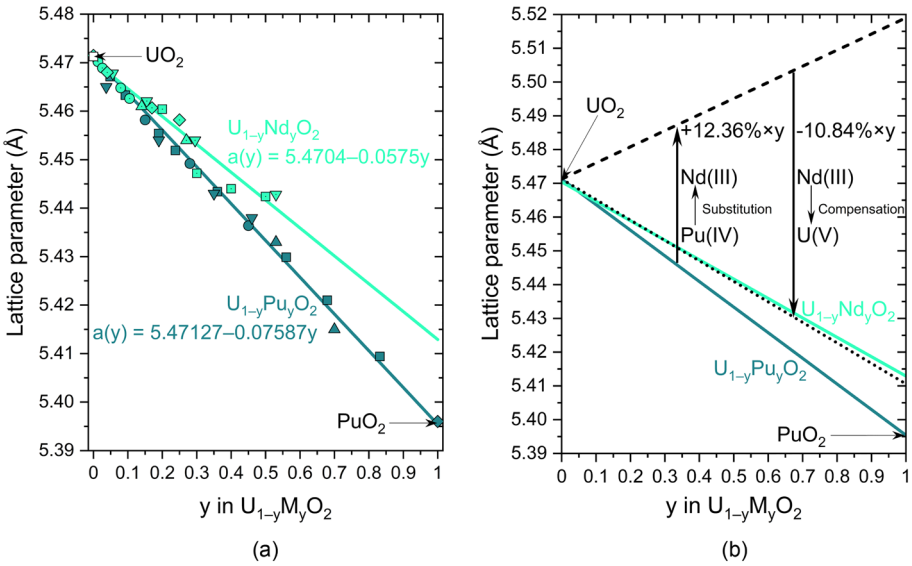

Figure 3. (**a**) Variations in the experimental lattice parameters of $U_{1-y}M_yO_2$ at room temperature as a function of *y* with M=Pu or Nd. The symbols correspond to the experimental data at room temperature, and the lines to their linear regression as a function of *y* (Vegard's law). (**b**) Comparison of experimental (solid lines) and calculated lattice parameters from the tabulated ionic radii without (dashed line) and with (dotted line) the Nd(III)/U(V) compensation mechanism. N.B. the fit of $a_{U_{1-y}Nd_yO_2}(y)$ was extrapolated to $y = 1$ for the discussion, even if the fluorite structure is not maintained at high Nd concentrations.

Am(III)/Am ratio remains to be determined. In pure americium dioxide, the r_{cation}/r_{anion} is smaller than Pauling's geometrical limit (Table 1), and the anions should touch and form a close-pack arrangement. Since the lattice parameter of AmO_2 at room temperature is 5.3755(5) Å[16], the ionic radius of O(–II) in this compound is 1.344 Å, and gives, using Eq. (2), the revised cation radius of $r_{Am(IV)} = 0.984$ Å (for C.N. = 8). The ionic radius of Am(III) in eightfold coordination is taken from Cross[42] and equal to 1.108 Å.

From these ionic radii and by using the same method as above, the variations in the lattice parameters of $U_{1-y}\{Pu_{1-\alpha}[Am(IV)_{1-\beta}Am(III)_{\beta}]_{\alpha}\}_yO_2$ as a function of plutonium, americium, and Am(III)/Am contents can be calculated using Eq. (4).

$$a_{U_{1-y}\left\{Pu_{1-\alpha}\left[Am(IV)_{1-\beta}Am(III)_{\beta}\right]_{\alpha}\right\}_yO_2}(y,\alpha,\beta) = \frac{4}{\sqrt{3}} \times \left[\left(1-y-\beta\cdot\alpha\cdot y\right) \times r_{U(IV)} + (1-\alpha) \times y \times r_{Pu(IV)} + (1-\beta) \times \alpha \times y \times r_{Am(IV)} + \beta \times \alpha \times y \times r_{Am(III)} + \beta \times \alpha \times y \times r_{U(V)} + r_{O(-II)U-Pu-Am}(y,\alpha,\beta)\right] \quad (4)$$

with the oxygen ionic radius $r_{O(-II)U-Pu-Am}(y,\alpha,\beta)$ calculated in the same manner as for the Nd-doped UO_2.

Deviation from stoichiometry in fluorite-structured oxides

In addition to their ability to form solid solutions, the fluorite structure (oxides) can accommodate large deviations from stoichiometry[7,16,43]. We enlarged our hybrid model to nonstoichiometric materials. In oxygen-hypostoichiometric fluorite-structured dioxides (Oxygen/Metal < 2), Kim[44] and Chatzichristodoulou[45] have envisaged a flexible oxygen vacancy size but considered a fixed ionic oxygen radius. Since hypostoichiometry corresponds to removing anions from the crystal, the associated reduced cations' coordination number should, theoretically, be modified likewise (Fig. 1). However, due to the Born–Haber energy, the lattice does not collapse, therefore, we considered the oxygen vacancies as spherical entities instead of empty voids. The coordination number of the cations remains unchanged and equal to 8.

For discussion, we examined the fluorite-structured hypostoichiometric uranium–plutonium mixed oxides $U_{1-y}Pu_yO_{2-x}$ for which an empirical relation between the experimental lattice parameters (in Å) and deviations from stoichiometry at room temperature[31,46] exists. It is updated in Eq. (5) from the recent measurements of the accurate lattice parameters of UO_2[15] and PuO_2[16].

$$a_{U_{1-y}Pu_yO_{2-x}}(y,x) = a_{UO_2} + \frac{a_{PuO_2} - a_{UO_2}}{1-0} \times y + 0.32 \times x = 5.47127 - 0.07587 \times y + 0.32 \times x \quad (5)$$

In $U_{1-y}Pu_yO_{2-x}$, Pu(IV) can be partially reduced to Pu(III) and is solely responsible for the hypostoichiometry in the mixed oxide below ~ 1700 K. Due to the solid's electroneutrality, the deviation from stoichiometry x is directly correlated to the valence of the constitutive cations. If we simplify the system by focusing on the PuO_{2-x} dioxide (so $U_{1-y}Pu_yO_{2-x}$ with y = 1) and considering that the oxygen vacancies are doubly charged and balanced by two Pu(III), PuO_{2-x} can be defined as $Pu(IV)_{1-2x}Pu(III)_{2x}O_{2-x}$. Since tetra- and trivalent Pu have different ionic radii in the eightfold coordination, PuO_{2-x} will be treated as a solid solution of the hypothetical $Pu(IV)O_2$–$Pu(III)O_2$ system (even if the second end member has no physical meaning). Before estimating the oxygen vacancy's effective size in PuO_{2-x}, the oxygen ionic radius $r_{O(-II)}$ must be determined. Therefore, the ionic radius of Pu(III) in the eightfold coordination, taken from Cross[42] and equal to 1.112 Å, is implanted in the lower boundary of Pauling's first rule, $0.732 = r_{cation}/r_{anion}$ (for C.N. = 8), to calculate the anion's radius in the hypothetical $Pu(III)O_2$ dioxide. Figure 4a plots the variations in the ionic radius of oxygen as a function of y in $Pu(IV)_{1-y}Pu(III)_yO_2$. Equation (2) is then derived to obtain Eq. (6).

$$r_{V_{O(-II)PuO_{2-x}}}(x) = \frac{a_{PuO_{2-x}}(x) \times \sqrt{3}}{2 \times x} + \frac{4 \times x - 2}{x} \times r_{Pu(IV)} - 4 \times r_{Pu(III)} - \frac{2-x}{x} \times r_{O(-II)Pu(IV)-Pu(III)} \quad (6)$$

where $r_{V_{O(-II)PuO_{2-x}}}$ and $r_{O(-II)Pu(IV)-Pu(III)}$ (from Fig. 4a) are the effective sizes of the anion vacancy and the ionic radius of oxygen in $Pu(IV)_{1-y}Pu(III)_yO_2$, respectively. Figure 4b shows the variations in $r_{V_{O(-II)PuO_{2-x}}}$ as a function of the deviation from stoichiometry x and the lattice parameter of PuO_{2-x} at room temperature, from combining Eqs. (5) and (6).

These results confirm that the oxygen, vacancy's effective size is not constant, likewise the ionic radius of oxygen, and it depends on the dopant's concentration, here Pu(III), and rapidly decreases and stabilizes with the increasing deviation from stoichiometry.

We believe this method can be used for more complex systems, including solid solutions and/or compounds with aliovalent cations, such as plutonium in PuO_{2-x}.

Conclusions

This innovative method cleaves with the globally adopted model of ionic radii only depending on the constitutive species' oxidation state and coordination number. Using simple structures, such as fluorites and antifluorites, we break the hard-sphere model by demonstrating that the anions are soft because their radius varies with the nature (size) of the surrounding cations. This hybrid model does not violate Pauling's first rule and can predict the lattice parameters of new fluorite and antifluorite-structured solid solutions if the pure poles are known, as long as the host and dopant metal atoms have similar electronegativities. Finally, this geometrical method's transposition is possible to investigate the deviations from stoichiometry. This result confirms that, in hypostoichiometry, the oxygen vacancy's effective size will not be considered constant and depends on the doping species' nature and concentration. We also reasonably envisage that this method could be used for any ionic crystal.

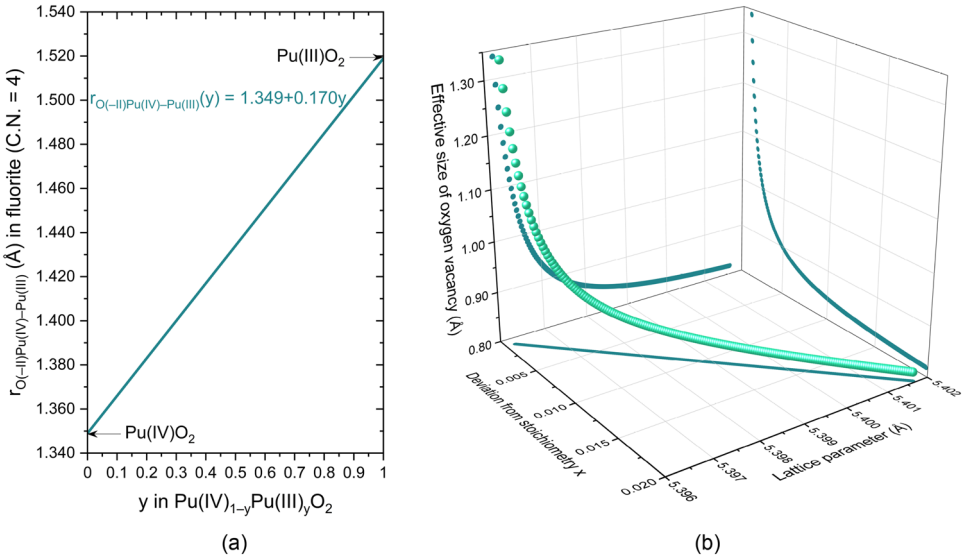

Figure 4. Variations in (**a**) the ionic radius of oxygen, noted $r_{O(-II)Pu(IV)-Pu(III)}$, as a function of y in the hypothetical $Pu(IV)_{1-y}Pu(III)_yO_2$ dioxide and (**b**) in the effective size of the oxygen vacancy as a function of the deviation from stoichiometry and the lattice parameter of PuO_{2-x} at room temperature. N.B. *x* was only set up to 0.02 because $PuO_{1.98}$ is the more reduced composition plutonium dioxide can reach without changing its structure at room temperature, i.e., without forming a second phase.

Data availability

All data generated or analyzed during this study are included in this published article and its supplementary information files.

Received: 15 December 2022; Accepted: 2 February 2023
Published online: 08 February 2023

References

1. Shannon, R. D. Revised effective ionic radii and systematic studies of interatomic distances in halides and chalcogenides. *Acta Crystallogr. A* **32**, 751–767 (1976).
2. Pauling, L. The principles determining the structure of complex ionic crystals. *J. Am. Chem. Soc.* **51**, 1010–1026 (1929).
3. Shannon, R. D. & Prewitt, C. T. Effective ionic radii in oxides and fluorides. *Acta Crystallogr. B* **25**, 925–946 (1969).
4. Kato, M. & Konashi, K. Lattice parameters of (U, Pu, Am, Np)O_{2-x}. *J. Nucl. Mater.* **385**, 117–121 (2009).
5. Xing, F., Ma, J., Shimizu, K. & Furukawa, S. High-entropy intermetallics on ceria as efficient catalysts for the oxidative dehydrogenation of propane using CO_2. *Nat. Commun.* **13**, 5065 (2022).
6. Kuganathan, N., Iyngaran, P. & Chroneos, A. Lithium diffusion in Li_5FeO_4. *Sci. Rep.* **8**, 5832 (2018).
7. Sickafus, K. E. *et al.* Radiation-induced amorphization resistance and radiation tolerance in structurally related oxides. *Nat. Mater.* **6**, 217–223 (2007).
8. Klein, C. & Dutrow, B. *Manual of Mineral Science* (John Wiley & Sons, 2007).
9. Haynes, W. M. *CRC Handbook of Chemistry and Physics* (CRC Press, 2014). https://doi.org/10.1201/b17118.
10. Ploc, R. A. The lattice parameter of cubic ZrO_2 formed on zirconium. *J. Nucl. Mater.* **99**, 124–128 (1981).
11. Gruen, D. M., Koehler, W. C. & Katz, J. J. Higher oxides of the lanthanide elements. Terbium dioxide. *J. Am. Chem. Soc.* **73**, 1475–1479 (1951).
12. Hong, Q.-J. *et al.* Combined computational and experimental investigation of high temperature thermodynamics and structure of cubic ZrO_2 and HfO_2. *Sci. Rep.* **8**, 14962 (2018).
13. Vauchy, R. *et al.* Liquid phase sintering of alumina–silica co-doped cerium dioxide CeO_2 ceramics. *Ceram. Int.* **49**, 3058–3065 (2023).
14. Vauchy, R. *et al.* New sample stage for characterizing radioactive materials by X-ray powder diffraction: Application on five actinide dioxides ThO_2, UO_2, NpO_2, PuO_2 and Am_O2. *J. Appl. Crystallogr.* **54**, 636–643 (2021).
15. Leinders, G., Cardinaels, T., Binnemans, K. & Verwerft, M. Accurate lattice parameter measurements of stoichiometric uranium dioxide. *J. Nucl. Mater.* **459**, 135–142 (2015).
16. Vauchy, R., Joly, A. & Valot, C. Lattice thermal expansion of $Pu_{1-y}Am_yO_{2-x}$ plutonium–americium mixed oxides. *J. Appl. Crystallogr.* **50**, 1782–1790 (2017).
17. Noé, M. & Fuger, J. Self-radiation effects on the lattice parameter of $^{244}CmO_2$. *Inorg. Nucl. Chem. Lett.* **7**, 421–430 (1971).
18. Fahey, J. A., Turcotte, R. P. & Chikalla, T. D. Thermal expansion of the actinide dioxides. *Inorg. Nucl. Chem. Lett.* **10**, 459–465 (1974).
19. Baybarz, R. D. & Haire, R. G. Investigation of the transplutonium oxides by X-ray and electron diffraction. *J. Inorg. Nucl. Chem.* 7–12 (1976).
20. Scheidecker, R. & Berard, M. F. Interdiffusion in the system CaF_2–SrF_2. *J. Am. Ceram. Soc.* **56**, 204–206 (1973).
21. Deadmore, D. L. & Sliney, H. E. *Hardness of CaF_2 and BaF_2 Solid Lubricants at 25 to 670 °C*. (1987).
22. Begun, G. M., Haire, R. G., Wilmarth, W. R. & Peterson, J. R. Raman spectra of some actinide dioxides and of EuF_2. *J. Common Met.* **162**, 129–133 (1990).
23. Popov, P. A. *et al.* Thermal conductivity and expansion of PbF_2 single crystals. *Ionics* **23**, 233–239 (2017).

24. Wu, X. *et al.* High pressure X-ray diffraction study of sodium oxide (Na2O): Observations of amorphization and equation of state measurements to 15.9 GPa. *J. Alloys Compd.* **823**, 153793 (2020).
25. Tanifuji, T., Shiozawa, K. & Nasu, S. Heat capacity of lithium oxide from 306 to 1073 K. *J. Nucl. Mater.* **78**, 422–424 (1978).
26. Zintl, E., Harder, A. & Dauth, B. Gitterstruktur der oxyde, sulfide, selenide und telluride des lithiums, natriums und kaliums. *Z. Elektrochem. Angew. Phys. Chem.* **40**, 588–593 (1934).
27. Baidya, T. *et al.* Understanding the anomalous behavior of Vegard's law in $Ce_{1-x}M_xO_2$ (M = Sn and Ti; $0 < x \leq 0.5$) solid solutions. *Phys. Chem. Chem. Phys.* **18**, 13974–13983 (2016).
28. Epifano, E. *et al.* Extreme multi-valence states in mixed actinide oxides. *Commun. Chem.* **2**, 1–11 (2019).
29. Warshaw, I. & Roy, R. Polymorphism of the rare earth sesquioxides. *J. Phys. Chem.* **65**, 2048–2051 (1961).
30. Herrero, B. *et al.* Charge compensation mechanisms in Nd-doped UO_2 samples for stoichiometric and hypo-stoichiometric conditions: Lack of miscibility gap. *J. Nucl. Mater.* **539**, 152276 (2020).
31. Ohmichi, T., Fukushima, S., Maeda, A. & Watanabe, H. On the relation between lattice parameter and O/M ratio for uranium dioxide-trivalent rare earth oxide solid solution. *J. Nucl. Mater.* https://doi.org/10.1016/0022-3115(81)90544-4 (1981).
32. Vauchy, R., Hirooka, S., Matsumoto, T. & Kato, M. Cation interdiffusion in uranium–plutonium mixed oxide fuels: Where are we now?. *Front. Nucl. Eng.* **1**, 1–18 (2022).
33. Lyon, W. L. & Baily, W. E. The solid-liquid phase diagram for the UO_2–PuO_2 system. *J. Nucl. Mater.* **22**, 332–339 (1967).
34. Vauchy, R., Robisson, A.-C., Audubert, F. & Hodaj, F. Ceramic processing of uranium–plutonium mixed oxide fuels $(U_{1-y}Pu_y)O_2$ with high plutonium content. *Ceram. Int.* **40**, 10991–10999 (2014).
35. Sali, S. K., Kulkarni, N. K., Phatak, R. & Agarwal, R. Oxidation behaviour of plutonium rich (U, Pu)C and $(U, Pu)O_2$. *J. Nucl. Mater.* **479**, 623–632 (2016).
36. Elorrieta, J. M. *et al.* Raman study of the oxidation in $(U, Pu)O_2$ as a function of Pu content. *J. Nucl. Mater.* **495**, 484–491 (2017).
37. Wadier, J.-F. *Diagramme de Phases et Propriétés Thermodynamiques du Système Uranium-Néodyme-Oxygène* (Paris 6, 1973).
38. Une, K. & Oguma, M. Oxygen potentials of $(U, Nd)O_{2\pm x}$ solid solutions in the temperature range 1000–1500 °C. *J. Nucl. Mater.* **118**, 189–194 (1983).
39. Lee, S. M., Knight, T. W., Voit, S. L. & Barabash, R. I. Lattice parameter behavior with different Nd and O concentrations in $(U_{1-y}Nd_y)O_{2\pm x}$ solid solution. *Nucl. Technol.* **193**, 287–296 (2016).
40. Marchenko, E. I. *et al.* Transferable approach of semi-empirical modeling of disordered mixed-halide hybrid perovskites $CH_3NH_3Pb(I_{1-x}Br_x)_3$: Prediction of thermodynamic properties, phase stability, and deviations from Vegard's law. *J. Phys. Chem. C* **123**, 26036–26040 (2019).
41. Vauchy, R. *et al.* Impact of the cation distribution homogeneity on the americium oxidation state in the $U_{0.54}Pu_{0.45}Am_{0.01}O_{2-x}$ mixed oxide. *J. Nucl. Mater.* **456**, 115–119 (2015).
42. Cross, J. N. *et al.* Syntheses, structures, and spectroscopic properties of plutonium and americium phosphites and the redetermination of the ionic radii of Pu(III) and Am(III). *Inorg. Chem.* **51**, 8419–8424 (2012).
43. Sørensen, O. T. Thermodynamics and defect structure of nonstoichiometric oxides. In *Nonstoichiometric Oxides* (ed. Sørensen, O. T.) 1–59 (Academic Press, 1981). https://doi.org/10.1016/B978-0-12-655280-5.50006-7.
44. Kim, D.-J. Lattice parameters, ionic conductivities, and solubility limits in fluorite-structure MO_2 oxide [M = Hf^{4+}, Zr^{4+}, Ce^{4+}, Th^{4+}, U^{4+}] solid solutions. *J. Am. Ceram. Soc.* **72**, 1415–1421 (1989).
45. Chatzichristodoulou, C., Norby, P., Hendriksen, P. V. & Mogensen, M. B. Size of oxide vacancies in fluorite and perovskite structured oxides. *J. Electroceram.* **34**, 100–107 (2015).
46. Vauchy, R. *et al.* Room-temperature oxidation of hypostoichiometric uranium–plutonium mixed oxides $U_{1-y}Pu_yO_{2-x}$—A depth-selective approach. *J. Nucl. Mater.* **465**, 349–357 (2015).
47. Momma, K. & Izumi, F. VESTA 3 for three-dimensional visualization of crystal, volumetric and morphology data. *J. Appl. Crystallogr.* **44**, 1272–1276 (2011).

Acknowledgements
The crystal structures were plotted with VESTA[47].

Author contributions
R.V. conceived the study, theorized the concept, analyzed the data, wrote, prepared, and revised the manuscript. R.V., S.H., M.W., and M.K. all discussed the theory and results. R.V., and S.H. edited the manuscript.

Competing interests
The authors declare no competing interests.

Additional information
Supplementary Information The online version contains supplementary material available at https://doi.org/10.1038/s41598-023-29326-0.

Correspondence and requests for materials should be addressed to R.V.

Reprints and permissions information is available at www.nature.com/reprints.

Publisher's note Springer Nature remains neutral with regard to jurisdictional claims in published maps and institutional affiliations.

Open Access This article is licensed under a Creative Commons Attribution 4.0 International License, which permits use, sharing, adaptation, distribution and reproduction in any medium or format, as long as you give appropriate credit to the original author(s) and the source, provide a link to the Creative Commons licence, and indicate if changes were made. The images or other third party material in this article are included in the article's Creative Commons licence, unless indicated otherwise in a credit line to the material. If material is not included in the article's Creative Commons licence and your intended use is not permitted by statutory regulation or exceeds the permitted use, you will need to obtain permission directly from the copyright holder. To view a copy of this licence, visit http://creativecommons.org/licenses/by/4.0/.

© The Author(s) 2023, corrected publication 2023